# Toroidal angular momentum balance during rotation changes induced by electron heating modulation in tokamak plasmas

Yasuhiro Idomura

Citation: Physics of Plasmas **24**, 080701 (2017); doi: 10.1063/1.4996017
View online: http://dx.doi.org/10.1063/1.4996017
View Table of Contents: http://aip.scitation.org/toc/php/24/8
Published by the American Institute of Physics

# Toroidal angular momentum balance during rotation changes induced by electron heating modulation in tokamak plasmas

Yasuhiro Idomura
*Japan Atomic Energy Agency, Wakashiba 178-4, Kashiwa, Chiba 277-0871, Japan*

(Received 29 April 2017; accepted 12 July 2017; published online 26 July 2017)

An electron heating modulation numerical experiment based on a global full-$f$ gyrokinetic model shows that transitions from ion temperature gradient driven (ITG) turbulence to trapped electron mode (TEM) turbulence induced by electron heating generate density peaking and rotation changes. Toroidal angular momentum balance during the rotation changes is revealed by direct observation of toroidal angular momentum conservation, in which in addition to ion turbulent stress, ion neoclassical stress, radial currents, and toroidal field stress of ions and electrons are important. Toroidal torque flipping between ITG and TEM phases is found to be related to reversal of the ion radial current, which indicates the coupling of particle and momentum transport channels. The ion and electron radial currents are balanced to satisfy the ambipolar condition, and the electron radial current is cancelled by the electron toroidal field stress, which indirectly affects toroidal torque. *Published by AIP Publishing.* [http://dx.doi.org/10.1063/1.4996017]

In toroidal magnetic confinement fusion devices, it is well known that the toroidal plasma rotation and its shear suppress turbulent energy transport[1] and magnetohydrodynamic instabilities.[2–4] In future large devices such as ITER, the auxiliary momentum input primary due to neutral beam injection (NBI) will be smaller than that in existing devices, and the self-organized toroidal angular momentum, called intrinsic rotation, is expected to dominate toroidal plasma rotation, which is sustained by various nondiffusive contributions to the toroidal angular momentum balance. The intrinsic rotation and its bifurcation behavior (spontaneous flipping of the toroidal plasma rotation with small changes in the plasma parameters) were experimentally observed, and their phenomenological understanding has been significantly advanced.[5–7] In addition, electron cyclotron resonance heating (ECRH) modulation experiments have indicated transient changes in intrinsic torque, suggesting the possibility of controlling the intrinsic rotation without momentum input.[8–10] It is crucial to understand the mechanism of rotation change in establishing such indirect rotation control.

In the ECRH modulation experiment on the ASDEX Upgrade tokamak,[9] prompt ($<$1 ms) electron heating as well as delayed ($\sim$10 ms) density peaking and rotation changes in the counter-current direction were induced after applying ECRH without additional particle or momentum input. The density peaking was well explained by quasilinear gyrokinetic calculations, which indicate the transition of dominant microinstabilities from the ion temperature gradient driven (ITG) mode to the trapped electron mode (TEM) and the resulting particle pinch or inward thermodiffusion.[11] However, the same quasilinear gyrokinetic calculations showed that with the density peaking, the inward momentum pinch due to the Colioris pinch[12] became significantly larger than the outward momentum diffusion, which is the opposite trend from that shown by experiment.[9] Therefore, the underlying mechanism of rotation changes induced by electron heating is still an open issue.

Theoretically, turbulent stress is often decomposed into diffusion, pinch, and residual stress, which come from turbulent momentum fluxes proportional to the gradient and the magnitude of toroidal rotation, as well as other nondiffusive contributions. Based on a symmetry breaking of turbulent spectra in the direction parallel to the magnetic field,[13,14] various pinch and residual stress models have been proposed; in addition, they have been verified by first principles based gyrokinetic calculations.[15] However, most former works were based on $\delta f$ calculations, which compute only the turbulent plasma distributions, $\delta f$, by assuming steady background distributions, $f_0$, and thus may not be valid for transient phenomena. In addition, in the toroidal angular momentum conservation law,[16–18] there exist several torque generation mechanisms other than the turbulent stress. Although neoclassical or collisional momentum transport is negligible in axisymmetric tokamak devices,[19] it can be comparable to the turbulent stress in the presence of non-axisymmetric turbulent perturbations.[20,21] The toroidal field stress[16] or the polarization stress[22] is induced by turbulent toroidal electric fields. In the presence of finite particle transport during transient density changes, the resulting $\mathbf{J} \times \mathbf{B}$ torque may be important. These mechanisms are not considered in $\delta f$ calculations. For understanding the complicated roles of the above momentum transport processes, one needs comprehensive numerical experiments based on global full-$f$ models, which compute evolutions of both $f_0$ and $\delta f$ using the same gyrokinetic model, thus satisfying the toroidal angular momentum conservation law. First principles based gyrokinetic calculations of turbulent transport and transient plasma responses over $\sim$10 ms order are feasible with state-of-the-art full-$f$ simulations on petascale supercomputers.

In this letter, we report the first direct observation of the toroidal angular momentum conservation law in an electron heating modulation numerical experiment using the global full-$f$ gyrokinetic Eulerian code, GT5D.[23,24] The numerical experiment shows that (i) transitions from ITG turbulence to

TEM turbulence generate density peaking and rotation changes induced by electron heating modulation; (ii) in addition to the ion turbulent stress, the ion neoclassical stress, radial currents, and toroidal field stress significantly contribute to the toroidal angular momentum balance; and (iii) toroidal torque flipping between the ITG and TEM phases is mainly attributed to reversal of the ion radial current, suggesting that the coupling between the particle and momentum transport channels plays a critical role.

We consider the electrostatic ITG-TEM turbulence in a circular concentric tokamak configuration with $R/a = 2.79$ and $q(r) = 0.85 + 2.18(r/a)^2$, with initial conditions close to the so-called Cyclone DIII-D base case[25] at the midradius $r_s = 0.5a$: $\epsilon = r_s/R \sim 0.18$, $q(r_s) \sim 1.4$, $\hat{s}(r_s) = [(r/q)dq/dr]_{r=r_s} \sim 0.78$, $n_e \sim 4.6 \times 10^{19}\mathrm{m}^{-3}$, $T_e \sim T_i \sim 2\mathrm{keV}$, $R/L_n = 2.22$, and $R/L_{ti} = R/L_{te} = 6.92$. Here, $a$ is the minor radius, $R$ is the major radius, $q$ is the safety factor, $\epsilon$ is the local inverse aspect ratio, $n_e$ is the electron density, $T_e$ and $T_i$ are the electron and ion temperature, and $L_n$, $L_{te}$, and $L_{ti}$ are the scale lengths of $n_e$, $T_e$, and $T_i$, respectively. The normalized electron and ion collisionality parameters at $r = r_s$ are $\nu_{*e} = (4/3\sqrt{\pi})qR\hat{\nu}_{ei}/v_{Te} \sim 0.034$ and $\nu_{*i} = (2\sqrt{2}/3\sqrt{\pi})qR\hat{\nu}_{ii}/v_{Ti} \sim 0.024$, respectively, where $\hat{\nu}_{ab} = (2\pi n_b q_b^2 q_a^2 \ln\Lambda_{ab})/(\sqrt{2}m_a^2 v_{Ta}^3)$, $v_{Ta} = \sqrt{T_a/m_a}$, and $\Lambda_{ab}$ is the Coulomb logarithm. The initial density gradient and the initial temperature ratio are close also to the plasma parameters $R/L_n \sim 2$ and $T_e/T_i = 1$ observed before applying electron heating in the ECRH modulation experiment.[9,11] To facilitate a long time numerical experiment over $\sim 20\,\mathrm{ms}$ ($\sim 4361\,R/v_{ti}$), we use the hybrid electron model[24] with a mass ratio of $m_i/m_e = 100$, and the plasma size parameter is reduced to $a/\rho_{ti} = 150$, where $\rho_{ti}$ is the ion Larmor radius evaluated using the volume averaged thermal velocity $v_{ti}$. It is noted that the reduced mass ratio of $m_i/m_e = 100$ could lead to a few per cent errors in the linear growth rate of TEM in the collisionless limit.[26] $\nu_{*e}$ and thus basic properties of electron neoclassical transport are unaffected by the mass ratio. However, the collisional stabilization of TEM, which depends on the ratio of $\hat{\nu}_{ei}$ to $R/v_{ti}$, is underestimated, and therefore, the evolutions of electron temperature profiles may be limited to lower $R/L_{te}$ and $T_e/T_i$ compared to the experiment. GT5D computes ion scale turbulence based on the standard first order (in $\rho_{ti}/a$) gyrokinetics, which satisfy the toroidal angular momentum conservation law. It is noted that, in the limit of ion scale turbulence, higher order corrections to the toroidal angular momentum conservation law are negligible.[17] Although the experiment was driven by NBI, for simplicity, we use an auxiliary heating model given by isotropic velocity space deposition with no particle or momentum input; its radial deposition profile is distributed in the plasma core ($r/a < 0.4$). A sink model is given by a Krook operator near the plasma surface ($r/a > 0.9$), which fixes the edge density, temperature, and rotation on average to the initial values with a time constant of $\tau_s = 10a/v_{ti}$, and thus, it works also as a particle and momentum source. The gyrokinetic equation is computed using the non-dissipative and conservative finite difference scheme,[23] which avoids the growth of numerical oscillations by conserving both $f$ and $f^2$, and thus, we do not use any grid-scale dissipation. On the other hand, turbulent fields are treated using the field-aligned Poisson solver,[27] which avoids high $k_\parallel$ noise and aliasing effects. A 1/6 wedge torus is resolved using $(N_R, N_\varphi, N_Z, N_{v\parallel}, N_{v\perp}) = (160, 32, 160, 96, 20)$ grid points, where $\mathbf{R} = (R, \varphi, Z)$ are the cylindrical coordinates, and $v_\parallel$ and $v_\perp$ are the velocities in the directions parallel and perpendicular to the magnetic field, respectively. Here, the maximum velocity and wave number are given as $v_{\parallel,max} = \pm 6v_{ts}$, $v_{\perp,max} = 5v_{ts}$ and $k_{R,max}\rho_{ti} = k_{Z,max}\rho_{ti} \sim 1.6$, $n_{max} = 48$ ($k_{\theta,max}\rho_{ti} \sim 0.9$ at $r = r_s$), respectively. The numerical parameters are chosen based on verification studies of neoclassical transport, zonal flow damping, and ITG-TEM stability, as well as nonlinear convergence studies including kinetic electrons.[24] It is noted that Ref. 11 showed that dominant turbulent fluxes come from $k_\theta\rho_{ti} < 0.5$ in both heating phases with and without ECRH, which can be covered by the above numerical resolution. In the numerical experiment, $\sim 10^6$ time steps are integrated with a time step width of $\Delta t = 0.013a/v_{ti}$, which costs $\sim 10^7$ CPU hours on the K-computer.

The time evolutions of the numerical experiment are shown in Fig. 1. In the initial condition, the ITG mode is

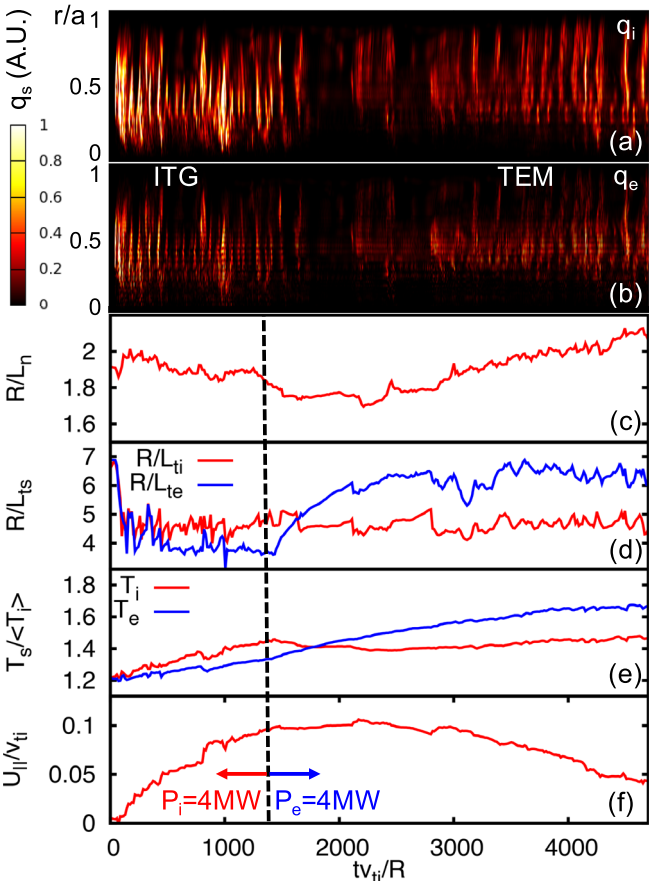


FIG. 1. An electron heating modulation numerical experiment using GT5D. Temporal and radial evolutions of (a) ion and (b) electron heat fluxes, $q_i$ and $q_e$, respectively. The time histories of (c) the normalized density gradient $R/L_n$, (d) the normalized ion and electron temperature gradients, $R/L_{ti}$ and $R/L_{te}$, respectively, (e) the ion and electron temperature, $T_i$ and $T_e$, respectively, normalized by the volume averaged initial temperature, $\langle T_i \rangle$, and (f) the flux-surface averaged parallel flow, $U_\parallel$, normalized by the ion thermal velocity, $v_{ti}$, are observed at $r \sim 0.5a$. The heating condition is switched from ion heating to electron heating at $t \sim 1400\,R/v_{ti}$.

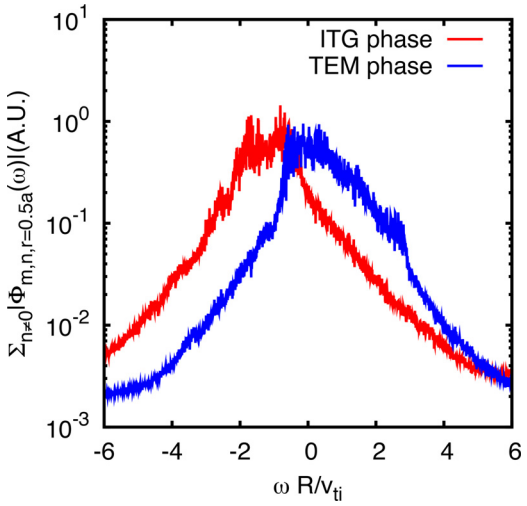


FIG. 2. The frequency spectra of the electrostatic potential at $r=0.5a$ in the ITG phase ($t=470$–$1400\,R/v_{ti}$) and the TEM phase ($t=3270$–$4600\,R/v_{ti}$).

linearly unstable, the parallel flow is set to be zero ($U_\parallel=0$), and the ion heating condition, $P_i=4\,\mathrm{MW}$, $P_e=0$, is imposed, where $P_s$ denotes the heating power of the species $s$. Under the fixed flux condition, the ITG turbulence shows radially nonlocal avalanche like transport for both ions and electrons ((a) and (b)). Here, the electron temperature is sustained by the equipartition process through the zeroth order collision operator.[24] The ion heating phase (ITG phase) evolves into the quasi-steady state, where the density gradient parameter slightly decreases to $R/L_n\sim1.9$ and the co-current intrinsic rotation with $U_\parallel/v_{ti}\sim0.1$ is developed ((c) and (f)). At $t\sim1400\,R/v_{ti}$, the heating condition is switched to electron heating with the same heating power, $P_i=0$ and $P_e=4\,\mathrm{MW}$. By applying the electron heating, $R/L_{te}$ and $T_e/T_i$ are quickly increased ((d) and (e)), and the turbulent frequency spectra clearly show the transition from the ion diamagnetic direction $\omega<0$ to the electron diamagnetic direction $\omega>0$ (see Fig. 2). This indicates the onset of the TEM turbulence, which also shows radially nonlocal avalanche like transport as in the ITG phase ((a) and (b)). During the electron heating phase (TEM phase), the density gradient is gradually increased, and the parallel flow changes in the counter-current direction ((c) and (f)). It is noted that in both the ITG and TEM phases, neoclassical particle transport is outward, and thus, the density peaking can be attributed to turbulent inward thermodiffusion as already discussed in Ref. 11. These results are qualitatively consistent with the experiment.[9] However, the radial profiles in Fig. 3 show several quantitative differences. Because of the lack of particle and momentum sources, the density change in the plasma core is smaller than the experiment, and the intrinsic rotation in the ITG phase is not peaked in the plasma core. In the TEM phase, the temperature ratio is smaller than that observed in the experiment, which may be explained by less collisional TEM stabilization due to the reduced mass ratio.

The rotation change is analyzed based on the toroidal angular momentum conservation law[24]

$$\sum_{s=e,i}\left[\left\langle\frac{\partial m_s v_\parallel b_\varphi f_s}{\partial t}\right\rangle+\left\langle\frac{1}{\mathcal{J}}\frac{\partial}{\partial\mathbf{R}}\cdot\left(\mathcal{J}\dot{\mathbf{R}}m_s v_\parallel b_\varphi f_s\right)\right\rangle\right.$$
$$+\left\langle f_s\frac{\partial\Phi_s}{\partial\varphi}\right\rangle-\left\langle\frac{q_s}{c}f_s\dot{\mathbf{R}}\cdot\nabla\psi\right\rangle$$
$$\left.-\langle m_s v_\parallel b_\varphi C_s\rangle-\langle m_s v_\parallel b_\varphi S_s\rangle\right]=0,\qquad(1)$$

where $f_s$, $q_s$, and $m_s$ are the gyrocenter distribution, charge, and mass of the particle species $s$, respectively. $\psi$ is the poloidal flux, $\varphi$ is the toroidal angle, $\mathcal{J}$ is the Jacobian, $b_\varphi$ is the covariant toroidal component of $\mathbf{b}=\mathbf{B}/|\mathbf{B}|$, $\mathbf{B}$ is the equilibrium magnetic field, $c$ is the speed of light, $\Phi_s$ is the gyro-averaged electrostatic potential, and $\langle\cdot\rangle$ denotes the velocity space integral and flux-surface average operator. Equation (1) shows that the toroidal torque is balanced with the stress term (the second term), the toroidal field stress term (the third term), the radial current term (the fourth term), the collision term, and the source term. In the stress and radial current terms, the equation of guiding center motion, $\dot{\mathbf{R}}=\mathbf{v}_E+\mathbf{v}_B$, comprises the $\mathbf{E}\times\mathbf{B}$ drift $\mathbf{v}_E$ and the magnetic drift $\mathbf{v}_B$, which induce turbulent and neoclassical transport, respectively. The toroidal field stress term is generated by the phase difference between the density fluctuation $\delta n_s$ and the toroidal electric field fluctuation $\partial_\varphi\Phi_s$, which is small with adiabatic electrons satisfying $\delta n_e=q_e n_e\Phi_e/T_e$ but becomes significant with kinetic trapped electrons.[24] This term is interpreted as the off-

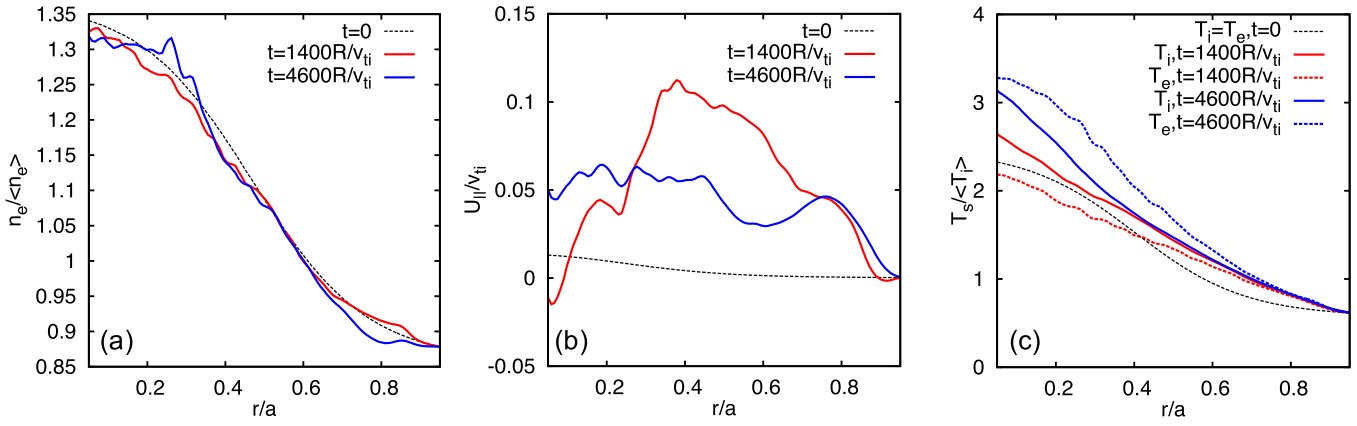


FIG. 3. The radial profiles of (a) the electron density $n_e$, (b) the flux-surface averaged parallel flow $U_\parallel$, and (c) the temperatures, $T_e$ and $T_i$, observed at the end of the ITG phase ($t=1400\,R/v_{ti}$) and the TEM phase ($t=4600\,R/v_{ti}$), respectively.

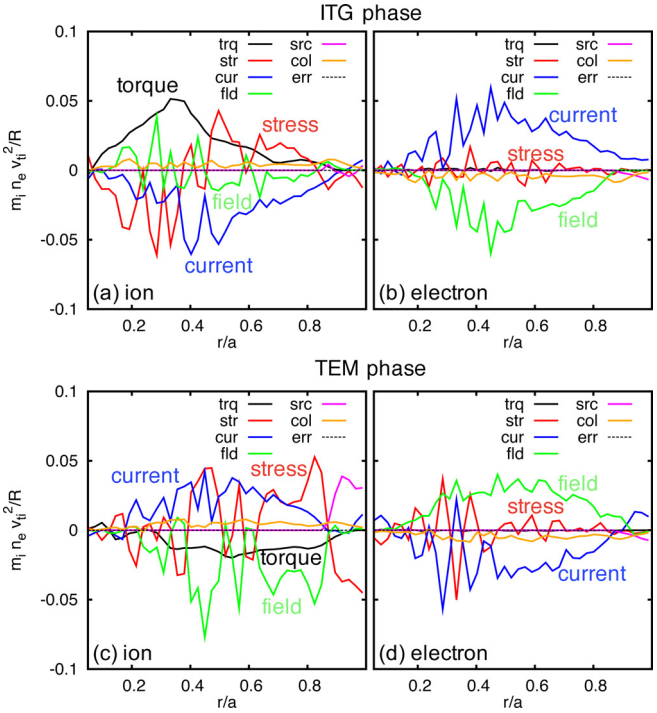


FIG. 4. The toroidal angular momentum balance in the ITG phase [$t = 470$–$1400\,R/v_{ti}$, (a) and (b)] and the TEM phase [$t = 3270$–$4600\,R/v_{ti}$, (c) and (d)] is observed for ions [(a) and (c)] and electrons [(b) and (d)]. The time averaged radial profiles of the toroidal torque (trq), stress term (str), radial current term (cur), toroidal field stress term (fld), source term (src), collision term (col), and the remaining error (err) are shown.

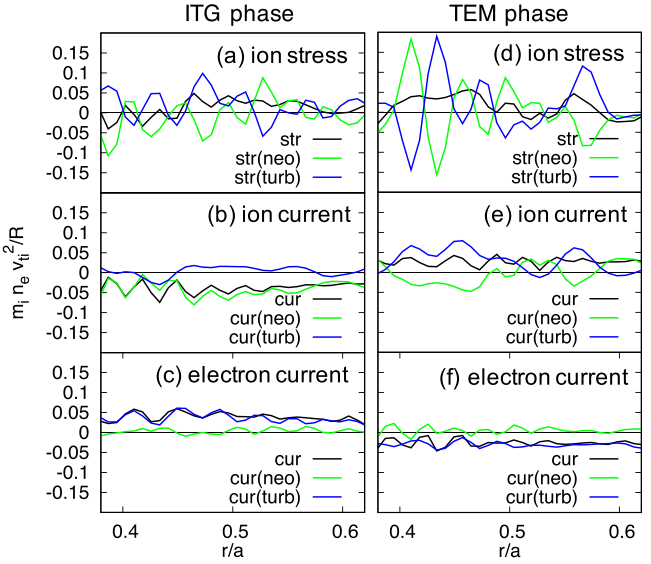


FIG. 5. The ion stress term [(a) and (d)], the ion radial current term [(b) and (e)], and the electron radial current term [(c) and (f)] in the ITG phase [(a)–(c)] and the TEM phase [(d)–(f)] in Fig. 4 are decomposed into neoclassical and turbulent components induced by the $\mathbf{E}\times\mathbf{B}$ and magnetic drifts, respectively.

diagonal electric component of the Maxwell stress tensor.[21] The radial current term satisfies the ambipolar condition,

$$-\frac{\rho_{ti}^2}{\lambda_{Di}^2}\frac{\partial E_\psi}{\partial t} = 4\pi\sum_{s=i,e} q_s\langle f_s\dot{\mathbf{R}}\cdot\nabla\psi\rangle, \tag{2}$$

where $\lambda_{Di}$ is the Debye length and $E_\psi = \mathbf{E}\cdot\nabla\psi$ is the radial electric field. It is noted that most of the earlier studies on intrinsic torque have focused only upon the ion stress term induced by turbulent transport; the contributions from neoclassical transport, the toroidal field stress term, the radial current term, and other contributions from the electron momentum balance, which is coupled with the ion momentum balance through the ambipolar condition and the collision operator, were not considered.

Figure 4 shows the toroidal angular momentum balance of ions and electrons in the ITG and TEM phases, which indicate co-current and counter-current toroidal torque, respectively, leading to rotation change. Numerical errors in the toroidal angular momentum balance are negligible. Because the source term due to the sink model is localized at the edge and the collision term is exactly cancelled between ions and electrons by the momentum conservation of the collision operator,[24] we focus upon the stress, toroidal field stress, and radial current terms. In the ion momentum balance, the stress and toroidal field stress terms tend to cancel each other, and the radial current term gives the main contribution to the toroidal torque. This indicates that the complicated transient plasma response is produced by coupling between the particle and momentum transport channels. The ion and electron radial current terms are balanced to satisfy the ambipolar condition (2). In the electron momentum balance, the toroidal torque and stress terms are negligible in the ion unit, $m_i n_e v_{ti}^2/R$, and thus, the radial current term is cancelled mainly by the toroidal field stress term. In Fig. 5, the ion stress term and the ion and electron radial current terms are further decomposed into neoclassical and turbulent components. In the ion stress term ((a) and (d)), the neoclassical and turbulent components are comparable and tend to cancel each other. This feature was also observed in ITG turbulence simulations with adiabatic electrons[20,21] and was predicted also by analytic calculations.[28] Although the ion radial current term [(b) and (e)] has similar features, the electron radial current term [(c) and (f)] is dominated by the turbulent component. This indicates that, unlike the conventional theory in which neoclassical and turbulent transport processes and their ambipolar conditions are considered independently by assuming scale separation, there exist multi-scale interactions between them, and the ambipolar condition is established including both processes. It is noted that GT5D recovers the neoclassical theory and the related ambipolar condition in the axisymmetric limit, and the enhanced ion neoclassical component appears only in the presence of non-axisymmetric turbulent fluctuations. This mechanism is different from that of the neoclassical toroidal viscosity induced by static three dimensional magnetic configurations with non-axisymmetric perturbed fields.

In summary, this work presented the first direct measurement of the toroidal angular momentum conservation law through a first principles based electron heating modulation numerical experiment, wherein the transition from the ITG turbulence to the TEM turbulence generates density peaking and rotation changes. In the ion toroidal angular momentum balance, in addition to the turbulent stress term, the neoclassical stress, toroidal field stress, and radial current

terms are shown to be important. It is found that the stress and toroidal field stress terms tend to cancel each other and that the main contribution to the toroidal torque comes from the radial current term, which is reversed between the ITG and TEM phases. This indicates that coupling between the particle and momentum transport channels plays a critical role in the complicated transient plasma response. The ion and electron radial current terms are connected through the ambipolar condition, which is established including both the neoclassical and turbulent fluxes. In the electron toroidal momentum balance, the radial current term is cancelled by the toroidal field term, suggesting an indirect coupling between the toroidal torque and the electron toroidal field stress term. These findings shed new light on the picture of self-organized toroidal angular momentum, where the constraints such as the toroidal angular momentum conservation law and the ambipolar condition are of critical importance. In future works, we will address electron heating modulation numerical experiments with a larger mass ratio and plasma size and also with impurity ions.

This work was supported by the MEXT (Grant for Post-K priority issue No. 6: Development of Innovative Clean Energy and Grant No. 22866086), the NIFS collaborative research program (NIFS16KNST103), and the JT-60 collaborative research program. Computations were performed on the K-computer (hp170075,hp160208) at the Riken, the Helios at the IFERC, the Plasma Simulator at the NIFS, and the ICEX at the JAEA.

[1]K. H. Burrell, Phys. Plasmas **4**, 1499 (1997).
[2]A. Bondeson and D. J. Ward, Phys. Rev. Lett. **72**, 2709 (1994).
[3]M. Takechi, G. Matsunaga, N. Aiba, T. Fujita, T. Ozeki, Y. Koide, Y. Sakamoto, G. Kurita, A. Isayama, and Y. Kamada, and the JT-60 Team, Phys. Rev. Lett. **98**, 055002 (2007).
[4]H. Reimerdes, A. M. Garofalo, G. L. Jackson, M. Okabayashi, E. J. Strait, M. S. Chu, Y. In, R. J. L. Haye, M. J. Lanctot, Y. Q. Liu *et al.*, Phys. Rev. Lett. **98**, 055001 (2007).
[5]J. E. Rice, A. Ince-Cushman, J. S. deGrassie, L.-G. Eriksson, Y. Sakamoto, A. Scarabosio, A. Bortolon, K. H. Burrell, B. P. Duval, C. Fenzi-Bonizec *et al.*, Nucl. Fusion **47**, 1618 (2007).
[6]K. Ida and J. R. Rice, Nucl. Fusion **54**, 045001 (2014).
[7]Y. Camenen, C. Angioni, A. Bortolon, B. P. Duval, E. Fable, W. A. Hornsby, R. M. McDermott, D. H. Na, Y.-S. Na, A. G. Peeters, and J. E. Rice, Plasma Phys. Controlled Fusion **59**, 034001 (2017).
[8]M. Yoshida, Y. Sakamoto, H. Takenaga, S. Ide, N. Oyama, T. Kobayashi, and Y. Kamada, and the JT-60 Team, Phys. Rev. Lett. **103**, 065003 (2009).
[9]R. M. McDermott, C. Angioni, R. Dux, A. Gude, T. Pütterich, F. Ryter, and G. Tardini, and the ASDEX Upgrade Team, Plasma Phys. Controlled Fusion **53**, 035007 (2011).
[10]D. R. Ernst, K. H. Burrell, W. Guttenfelder, T. L. Rhodes, A. M. Dimits, R. Bravenec, B. A. Grierson, C. Holland, J. Lohr, A. Marinoni *et al.*, Phys. Plasmas **23**, 056112 (2016).
[11]C. Angioni, R. McDermott, E. Fable, R. Fischer, T. Pütterich, F. Ryter, and G. Tardini, and the ASDEX Upgrade Team, Nucl. Fusion **51**, 023006 (2011).
[12]A. G. Peeters, C. Angioni, and D. Strintzi, Phys. Rev. Lett. **98**, 265003 (2007).
[13]A. G. Peeters, C. Angioni, A. Bortolon, Y. Camenen, F. J. Casson, B. Duval, L. Fiederspiel, W. A. Hornsby, Y. Idomura, T. Hein *et al.*, Nucl. Fusion **51**, 094027 (2011).
[14]P. H. Diamond, Y. Kosuga, O. D. Gürcan, C. J. McDevitt, T. S. Hahm, N. Fedorczak, J. E. Rice, W. X. Wang, S. Ku, J. Kwon *et al.*, Nucl. Fusion **53**, 104019 (2013).
[15]X. Garbet, Y. Idomura, L. Villard, and T. H. Watanabe, Nucl. Fusion **50**, 043002 (2010).
[16]B. Scott and J. Smirnov, Phys. Plasmas **17**, 112302 (2010).
[17]Y. Idomura, Comput. Sci. Discovery **5**, 014018 (2012).
[18]H. Sugama, T. H. Watanabe, and M. Nunami, Phys. Plasmas **21**, 012515 (2014).
[19]F. L. Hinton and R. D. Hazeltine, Rev. Mod. Phys. **48**, 239 (1976).
[20]Y. Idomura, Phys. Plasmas **21**, 022517 (2014).
[21]J. Abiteboul, X. Garbet, V. Grandgirard, S. J. Allfrey, P. Ghendrih, G. Latu, Y. Sarazin, and A. Strugarek, Phys. Plasmas **18**, 082503 (2011).
[22]C. J. McDevitt, P. H. Diamond, Ö. D. Gürcan, and T. S. Hahm, Phys. Rev. Lett. **103**, 205003 (2009).
[23]Y. Idomura, H. Urano, N. Aiba, and S. Tokuda, Nucl. Fusion **49**, 065029 (2009).
[24]Y. Idomura, J. Comput. Phys. **313**, 511 (2016).
[25]A. M. Dimits, G. Bateman, M. A. Beer, B. I. Cohen, W. Dorland, G. W. Hammett, C. Kim, J. E. Kinsey, M. Kotschenreuther, A. H. Kritz *et al.*, Phys. Plasmas **7**, 969 (2000).
[26]A. Bottino, "Ecole Polytechnique Fédérale de Lausanne," Ph.D. thesis (Ecole Polytechnique Federale de Lausanne, 2004).
[27]S. Jolliet, B. F. McMillan, L. Villard, T. Vernay, P. Angelino, T. M. Tran, S. Brunner, A. Bottino, and Y. Idomura, J. Comput. Phys. **231**, 745 (2012).
[28]X. Garbet, Y. Asahi, P. Donnel, C. Ehrlacher, G. Dif-Pradalier, P. Ghendrih, V. Grandgirard, and Y. Sarazin, New J. Phys. **19**, 015011 (2017).